

Symmetric Image Registration

Peter Rogelj^{*}, Stanislav Kovačič

*University of Ljubljana, Faculty of Electrical Engineering,
Tržaska 25, 1000 Ljubljana, Slovenia*

Abstract

This paper presents an original non-rigid image registration approach, which tends to improve the registration by establishing a symmetric image interdependence. In order to gather more information about the image transformation it measures the image similarity in both registration directions. The presented solution is based on the interaction between the images involved in the registration process. Images interact through forces, which according to Newton's action-reaction law form a symmetric relationship. These forces may transform both of the images, although in our implementation one of the images remains fixed. The experiments performed to demonstrate the advantages of the symmetric registration approach involve the registration of simple objects, the recovery of synthetic deformation, and the inter-patient registration of real images of the head. The results show that the symmetric approach improves both the registration consistency and the registration correctness.

Key words: Non-rigid registration, similarity measure, symmetry, registration consistency, registration correctness.

1 Introduction

The aim of image registration is to find a transformation that puts two imaged anatomies into a spatial correspondence. Each anatomical point in the first anatomy is expected to have exactly one homologous point in the second anatomy. It is intuitively expected that a more correct registration is reflected in a higher image similarity, which is also a standard assumption of image

^{*} Corresponding author.

Email address: peter.rogelj@fe.uni-lj.si (Peter Rogelj).

registration procedures. However, this assumption is not always valid, as similarity measures compare images in terms of their appearance and cannot assess transformations that do not change them in this respect.

Let us suppose that the overall transformation consists of several transformation components, e.g., translation and rotation in the case of rigid registration, and local deformations in the case of non-rigid registration. Such transformation components might correspond to changes in the individual transformation parameters, such that the number of transformation components is equal to the dimensionality of the transformation. The problem arises when some of the components do not change the image’s appearance and therefore they cannot be assessed by measuring the image similarity. Although this phenomenon is rare for global/rigid cases, it is quite common for local/non-rigid cases. By increasing the dimensionality of the transformation the proportion of transformation components that cannot be assessed by measuring the similarity increases. This causes difficulties in non-rigid registration, as well as in its validation (Woods, 1999; Gee, 2000; Schnabel et al., 2003; Fitzpatrick, 2001).

One of the properties of similarity measurement is asymmetry. To illustrate the problem, let us assume we have two images, A and B , and some transformation \mathbf{T} . Let us compare the images after the transformation is applied. The situation is shown in Figure 1. By transforming image A using the transformation \mathbf{T} , image $\mathbf{T}A$ is obtained. Although the transformation \mathbf{T} does change the image A (note the difference between the grids of A and $\mathbf{T}A$), in our specific case the appearance of image A remains unchanged. Consequently, the transformation cannot be assessed by measuring the similarity S , as $S(\mathbf{T}A, B)$ equals $S(A, B)$. However, the same match, i.e., the same point-to-point image correspondence, can be obtained by transforming image B instead of image A , but using the inverse transformation \mathbf{T}^{-1} . In our example the obtained image $\mathbf{T}^{-1}B$ evidently differs from the initial image B . Thus, this transformation can be detected and assessed by measuring the similarity S , as $S(A, \mathbf{T}^{-1}B)$ differs from $S(A, B)$. This illustration shows that measuring the similarity in different directions, i.e., by transforming the other image to obtain the same match, makes it possible to assess the different transformation components.

The phenomenon of the asymmetry of a similarity measurement is important for image registration, because it causes differences between registration results obtained when registering images in different registration directions. The presence of such differences is known as inverse inconsistency and indicates an error in at least one of the registration directions.

To avoid the inconsistency and thereby improve the registration Christensen and Johnson (Christensen and Johnson, 2001) proposed *consistent image registration*. Here, images are jointly registered in both registration directions, while both of the registration processes are linked with an additional consis-

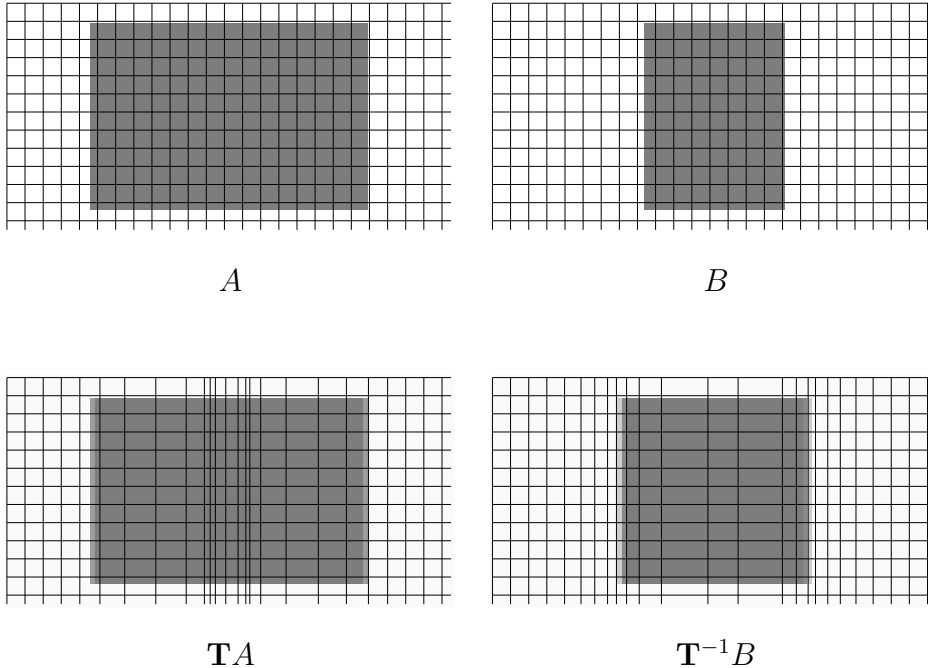


Fig. 1. Illustration of the similarity measure’s asymmetry. The measurement of similarity in different directions can assess the different transformation components. The transformations are shown by the deformation of the regular image grids. The similarity $S(\mathbf{T}A, B)$ does not differ from the similarity $S(A, B)$, which indicates that none of the transformation components present in transformation \mathbf{T} can be assessed by measuring the similarity in this registration direction. On the other hand, the same image correspondence as obtained by transforming image A using \mathbf{T} can also be obtained by transforming image B using \mathbf{T}^{-1} . This inverse transformation changes the appearance of image B such that the similarity $S(A, \mathbf{T}^{-1}B)$ differs from $S(A, B)$, which indicates that at least some transformation components can be assessed in this registration direction. The illustrated asymmetry is independent of the selection of the similarity measure used. In our particular case, using the overlap measure results in the following similarities: $S(\mathbf{T}A, B) = S(A, B) = 0.75$ and $S(A, \mathbf{T}^{-1}B) = 0.85$.

tency constraint. Another approach was proposed by Cachier and Rey (Cachier and Rey, 2000), whose *inversion invariant energies* symmetrize non-rigid registration in such a way that the overall criterion function becomes independent of the registration direction. Both solutions implicitly require measuring the similarity in both registration directions. However, in both cases this requires the computation of inverse transformations, which is a difficult and computationally complex task. Another interesting work was done by Ashburner et al. who symmetrized the probability distribution within the Bayesian Framework (Ashburner et al., 1999).

We propose an alternative registration approach, which does not force the consistency, but tackles the problem at its source by establishing a symmetric image interdependence. This makes it possible for the registration to gather

more information about the image transformation, as the image similarity is measured explicitly in both registration directions. The obtained registration results are consequently more correct as well as more consistent. In addition, the computational cost of the proposed approach is low and the computation of inverse transformations is not required.

2 Symmetric image registration

The symmetric registration approach treats both images involved in the registration process in the same manner. Both of the images share the same global coordinate system and can overlap. Both of the images can be modeled by spatial deformation models, possibly different ones, such that both of them can move and/or deform. Finally, the most distinctive feature of the symmetric registration approach is the interaction between the images. Images interact via forces in accordance with Newton’s third law of motion. Forces applied to one image are reflected in opposing forces on the other image, which forms the basis for the symmetry. The result of this interaction is a transformation of the images that puts the whole system into the equilibrium state of minimum energy.

Let A and B be the images involved in the registration. Each of them is defined in its own coordinate system, \mathbf{x}_A for image A and \mathbf{x}_B for image B . The images are mapped to the world coordinate system \mathbf{x} by the transformations \mathbf{T}_A and \mathbf{T}_B , such that $\mathbf{T}_A A$ and $\mathbf{T}_B B$ represent the transformed images as they appear in the global coordinate system \mathbf{x} . Here, the mappings of the image coordinates to the global coordinates are:

$$\mathbf{x} = \mathbf{x}_A + \mathbf{T}_A(\mathbf{x}_A), \quad (1)$$

$$\mathbf{x} = \mathbf{x}_B + \mathbf{T}_B(\mathbf{x}_B), \quad (2)$$

where $\mathbf{T}_A(\mathbf{x}_A)$ and $\mathbf{T}_B(\mathbf{x}_B)$ denote the displacements of points $A(\mathbf{x}_A)$ and $B(\mathbf{x}_B)$ from their initial (untransformed) positions.

Following a widely used gradient descent optimization algorithm, the external forces are defined as a gradient of image similarity $S(\mathbf{T}_A A, \mathbf{T}_B B)$. The forces F_A , which act on image A in order to match it with image B are then as follows:

$$\mathbf{F}_A = \frac{\partial S(\mathbf{T}_A A, \mathbf{T}_B B)}{\partial \mathbf{T}_A}. \quad (3)$$

In addition to image A , image B also tends to improve the matching. Forces

\mathbf{F}_B are exerted on image B in order to improve the matching of image B with image A :

$$\mathbf{F}_B = \frac{\partial S(\mathbf{T}_A A, \mathbf{T}_B B)}{\partial \mathbf{T}_B}. \quad (4)$$

The obtained forces, \mathbf{F}_A and \mathbf{F}_B , which we call forward forces, are not symmetric:

$$\mathbf{F}_A(\mathbf{x}) \neq -\mathbf{F}_B(\mathbf{x}). \quad (5)$$

Here, $\mathbf{F}_A(\mathbf{x})$ and $\mathbf{F}_B(\mathbf{x})$ denote forces at the same global coordinates \mathbf{x} . Note that the forces \mathbf{F}_A and \mathbf{F}_B act on different images. This asymmetry is a source of inverse inconsistency in the case of conventional non-rigid registration approaches. The forces \mathbf{F}_A and \mathbf{F}_B are actually estimated by measuring the similarity in different registration directions and so they are based on different information about the image transformation. Each of the gradients of similarity as defined in Eq. (3) and Eq. (4) depend only on the intensity gradient of one image. For example, if S is some global similarity measure, then the forces \mathbf{F}_A can differ from zero only at points with a non-zero gradient of image A , while the forces \mathbf{F}_B differ from zero at points with a non-zero gradient of image B . For an illustration of the forward forces see Figure 2.

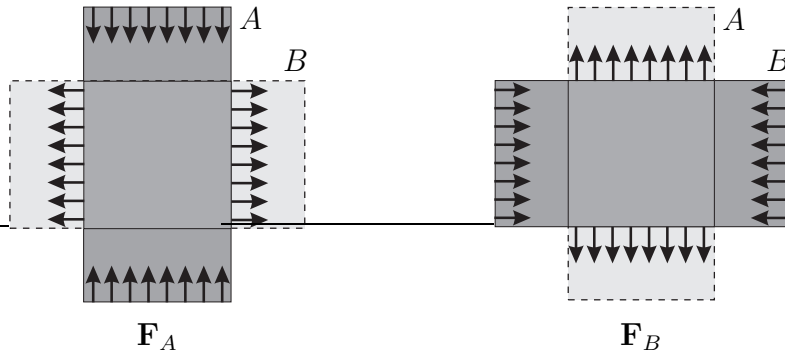


Fig. 2. Illustration of forces \mathbf{F}_A acting on image A (left) and forces \mathbf{F}_B acting on image B (right) when matching two rectangles. Note the asymmetry of the forces with respect to the registration direction, which is the main source of inconsistency with conventional registration procedures.

In contrast, the asymmetry does not affect the symmetric registration approach. In accordance with Newton's third law of motion, each force exerted in one of the images reflects in another force of the same magnitude that acts in the other image in the opposite direction. Thus, the forces \mathbf{F}_A reflect to forces \mathbf{F}'_A , which act on image B such that $\mathbf{F}'_A(\mathbf{x}) = -\mathbf{F}_A(\mathbf{x})$, and the forces \mathbf{F}_B reflect to forces \mathbf{F}'_B , which act on image A such that $\mathbf{F}'_B(\mathbf{x}) = -\mathbf{F}_B(\mathbf{x})$. The new forces are called reverse forces and are illustrated in Figure 3. The

resultant forces that act on image A are the sum of the forward and reverse forces:

$$\mathbf{F}^A(\mathbf{x}) = \mathbf{F}_A(\mathbf{x}) + \mathbf{F}'_B(\mathbf{x}) = \mathbf{F}_A(\mathbf{x}) - \mathbf{F}_B(\mathbf{x}), \quad (6)$$

and likewise the resultant forces on image B are

$$\mathbf{F}^B(\mathbf{x}) = \mathbf{F}_B(\mathbf{x}) + \mathbf{F}'_A(\mathbf{x}) = \mathbf{F}_B(\mathbf{x}) - \mathbf{F}_A(\mathbf{x}). \quad (7)$$

For an illustration of the resultant forces \mathbf{F}^A and \mathbf{F}^B see Figure 4.

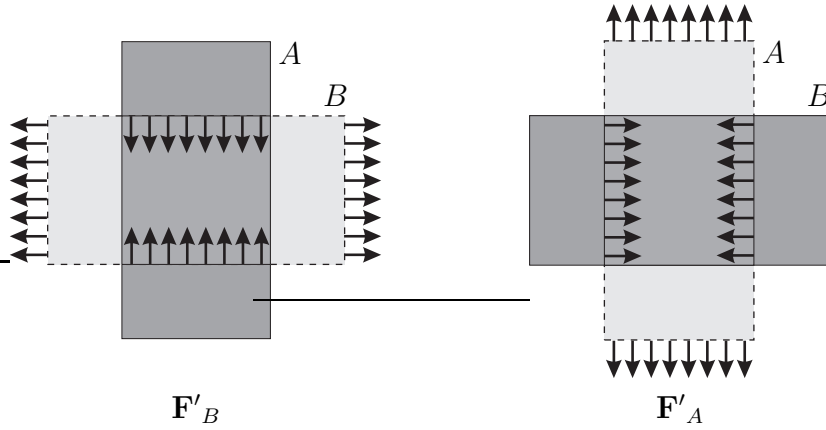


Fig. 3. Illustration of the reverse forces \mathbf{F}'_B acting on image A (left) and the reverse forces \mathbf{F}'_A acting on image B (right) when matching two rectangles.

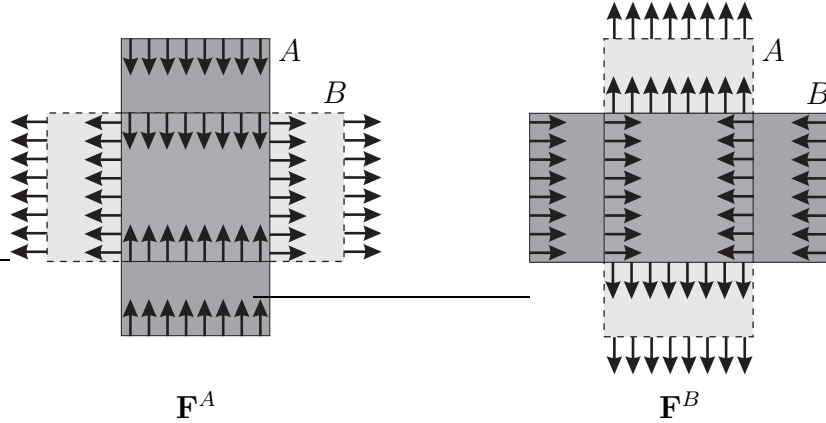


Fig. 4. Illustration of the symmetric forces \mathbf{F}^A acting on image A (left) and the symmetric forces \mathbf{F}^B acting on image B (right) when matching two rectangles. Note the increased amount of information available for transforming each of the images and the obtained symmetry $\mathbf{F}^A = -\mathbf{F}^B$, which is required for achieving the registration consistency.

The forces \mathbf{F}^A and \mathbf{F}^B are symmetric in the sense that they have the same magnitude but act on different images and in the opposite direction:

$$\mathbf{F}^A(\mathbf{x}) = -\mathbf{F}^B(\mathbf{x}). \quad (8)$$

When the symmetric forces are used for the registration, each of the resulting transformations, \mathbf{T}_A and \mathbf{T}_B , tend to correct the image differences in both directions, i.e., those that can be detected in one and those that can be detected in the opposite registration direction. Nevertheless, transformation \mathbf{T}_A can still be regularized with a different spatial deformation model than transformation \mathbf{T}_B , which presents us with new registration possibilities. In the case that the same spatial deformation model is used for both of the images, the registration is symmetric in all aspects and the registration results are absolutely consistent. However, it is often assumed that one of the images represents the undeformed configuration of the anatomy, while the other one is its deformed version. In this case better results are expected when transforming only one of the images, while the other image should remain untransformed. Consequently, images should be modeled by two different spatial deformation models. The target image A , which should not get transformed, must be fixed (modeled as a rigid body and anchored to the coordinate system), while the source image B must be modeled using a suitable deformable model. Note that although the target image is fixed, the forces \mathbf{F}_A still exist and they still contribute to the registration. Even if they cannot change the configuration of image A they still have an influence on the transformation of source image B . Therefore, the advantages of the symmetric registration approach remain and an improvement in the registration correctness can be expected.

2.1 Implementation details

In our implementation of registration we assume that only one of the images needs to be transformed (image B), while the other image (A) is fixed. However, the forces that drive the registration are obtained using the symmetric approach, such that the information of both registration directions is used.

For measuring the quality of the image match we use point-similarity measures (Rogelj et al., 2003), which are capable of estimating the similarity for individual image point pairs. They separate the process of measuring similarity into two steps. In the first step a point-similarity function $f(\mathbf{i})$, which is an estimation of image intensity dependence, is computed using the whole images. Here, $i = (i_A, i_B)$ denotes an image intensity pair. In the second step the similarity $S(\mathbf{x}_1, \mathbf{x}_2)$ of a point pair $(A(\mathbf{x}_1), B(\mathbf{x}_2))$ is computed from the corresponding intensity pair $\mathbf{i}(\mathbf{x}_1, \mathbf{x}_2) = (i_A(\mathbf{x}_1), i_B(\mathbf{x}_2))$ such that $S(\mathbf{x}_1, \mathbf{x}_2) = f(\mathbf{i}(\mathbf{x}_1, \mathbf{x}_2))$.

Due to point-similarity measures, we do not optimize the similarity of the whole images, but instead, the improvement of the image match is searched for by optimizing the similarities of individual image voxels. This is convenient for high dimensional registration, where transformation components correspond to the displacements of individual voxels. In this case an estimation of the ex-

ternal forces, which are also estimated for individual voxels, can be simplified, as each force $\mathbf{F}(\mathbf{x})$ depends only on one transformation component $\mathbf{T}(\mathbf{x})$ and not on the whole transformation (transformation of the whole image) \mathbf{T} .

The transformation \mathbf{T}_B , which transforms image B into image $\mathbf{T}_B B$, moves each point from its original (untransformed) position $\mathbf{x} = \mathbf{x}_B$ to a new position $\mathbf{x} = \mathbf{x}_B + \mathbf{T}_B(\mathbf{x}_B)$. Thus, the point at the global coordinate \mathbf{x} in image $\mathbf{T}_B B$, denoted $\mathbf{T}_B B(\mathbf{x})$, is in image B (according to its own image coordinate system) located at coordinates \mathbf{x}_B and denoted $B(\mathbf{x}_B)$:

$$\mathbf{T}_B B(\mathbf{x}) = B(\mathbf{x}_B), \quad (9)$$

The point $\mathbf{T}_B B(\mathbf{x})$ gets matched with point $\mathbf{T}_A A(\mathbf{x})$, but because image A is fixed ($\mathbf{T}_A(\mathbf{x}_A) = 0$) its image coordinates are equal to the global coordinates $\mathbf{x}_A = \mathbf{x}$, see eq.(1). Thus, at global coordinate \mathbf{x} , image point $\mathbf{T}_A A(\mathbf{x})$ matches with image point $\mathbf{T}_B B(\mathbf{x})$, such that

$$\mathbf{T}_A A(\mathbf{x}) = A(\mathbf{x}) = A(\mathbf{x}_B + \mathbf{T}_B(\mathbf{x}_B)). \quad (10)$$

This relationship can be used to compute the forward forces $\mathbf{F}_B(\mathbf{x})$:

$$\begin{aligned} \mathbf{F}_B(\mathbf{x}) &= \frac{\partial S(\mathbf{T}_A A(\mathbf{x}), \mathbf{T}_B B(\mathbf{x}))}{\partial \mathbf{T}_B} \\ &= \frac{\partial S(A(\mathbf{x}_B + \mathbf{T}_B(\mathbf{x}_B)), B(\mathbf{x}_B))}{\partial \mathbf{T}_B(\mathbf{x})}. \end{aligned} \quad (11)$$

The gradient of the point similarity can be computed numerically using similarities that correspond to the point displacements $\Delta \mathbf{T}_B(\mathbf{x}) = [-\varepsilon, 0, +\varepsilon]^3$ and form a $3 \times 3 \times 3$ point-similarity window, see Figure 5. Similarities for the points in image A that are not positioned on the image grid are interpolated from the similarities of neighboring grid points to obtain subvoxel accuracy and prevent interpolation artifacts (Rogelj and Kovačič, 2003). The further estimation of forces, i.e., gradients of similarity, follows Bajcsy and Kovačič (Bajcsy and Kovačič, 1989). Because point similarity measures rely on a global estimation of intensity dependence, an additional symmetrization of similarity window, such as proposed by Dengler (Dengler, 1986), is not needed.

For the computation of the reverse forces $\mathbf{F}'_A = -\mathbf{F}_A$, a gradient of similarity with respect to the transformation \mathbf{T}_A must be obtained. Although \mathbf{T}_A is in reality zero (image A is fixed) we need to compute how the similarity would change if the registration was performed in the opposite direction, using \mathbf{T}_A . In this case, point $A(\mathbf{x}_B + \mathbf{T}_B(\mathbf{x}_B))$ would no longer match with point $B(\mathbf{x}_B)$, but with some other point in image B , displaced from the coordinate \mathbf{x}_B by some displacement \mathbf{u} . To avoid any interpolation of image B , which is difficult

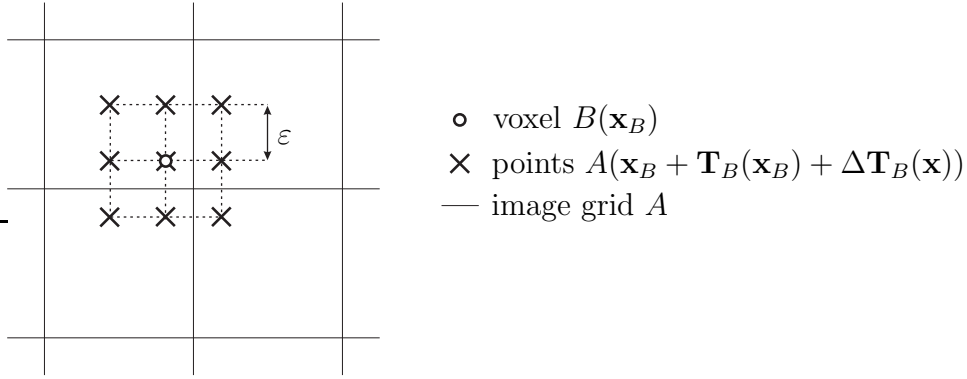


Fig. 5. 2D illustration of the points used for the estimation of forward forces \mathbf{F}_B .

because image B might be deformed, the gradient of similarity is numerically estimated by applying small displacements \mathbf{u} according to the coordinate system of image B , and not directly according to the global coordinate system:

$$\mathbf{F}_A(\mathbf{x}_B) = \left. \frac{\partial S(A(\mathbf{x}_B + \mathbf{T}_B(\mathbf{x}_B)), B(\mathbf{x}_B + \mathbf{u}))}{\partial \mathbf{u}} \right|_{\mathbf{u}=0}. \quad (12)$$

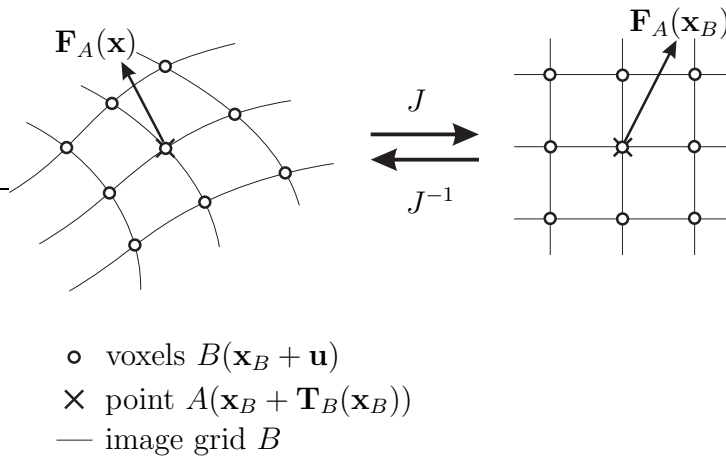


Fig. 6. 2D illustration of the points used for the numerical computation of reverse forces. The numerical derivation is performed in the coordinate system of image B and the result is mapped to the global coordinate system using a Jacobian matrix J .

Because the final reverse forces must be defined according to the global coordinate system \mathbf{x} , a local transformation between the global coordinate system \mathbf{x} and the image coordinate system \mathbf{x}_B must be obtained, see Figure 6. According to Eq. (2) the local transformation equals the Jacobian matrix J :

$$\frac{\partial \mathbf{x}}{\partial \mathbf{x}_B} = J = I + \frac{\partial \mathbf{T}(\mathbf{x}_B)}{\partial \mathbf{x}_B}, \quad (13)$$

$$\frac{\partial \mathbf{x}_B}{\partial \mathbf{x}} = J^{-1}. \quad (14)$$

Thus, the reverse forces defined in the global coordinate system are

$$\mathbf{F}_A(\mathbf{x}) = J^{-1}\mathbf{F}_A(\mathbf{x}_B). \quad (15)$$

When both sets of forces, \mathbf{F}_B and \mathbf{F}_A , are obtained, the resultant forces \mathbf{F}^B , used for registering image B to image A , are obtained as (7):

$$\mathbf{F}^B(\mathbf{x}) = \mathbf{F}_B(\mathbf{x}) - \mathbf{F}_A(\mathbf{x}). \quad (16)$$

3 Results

Three sets of experiments were performed to demonstrate the symmetric registration approach and compare it with mono-directional approaches. The experiments involved the registration of simple objects, the recovery of synthetic deformations, and the inter-patient registration of real images of a human head.

Each pair of images (A, B) used in the experiments was registered in both registration directions using the three different force-estimation approaches, i.e., one symmetric and two unidirectional. In total, six transformations were obtained for each image pair. The result of registering image B to image A using the forward forces \mathbf{F}_B , the reverse forces \mathbf{F}'_A and the symmetric forces \mathbf{F}^B were the transformations \mathbf{T}_F , \mathbf{T}_R and \mathbf{T}_S , respectively. When the registration was performed in the opposite direction, registering image A to image B , the transformations \mathbf{T}'_F , \mathbf{T}'_R and \mathbf{T}'_S were obtained, see Figure 7.

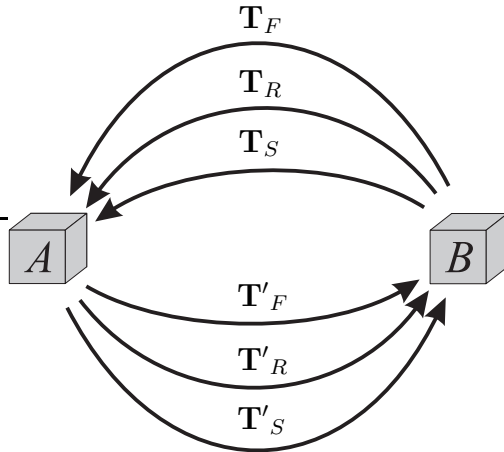


Fig. 7. Transformations obtained by registering images A and B , with respect to the method used for estimating forces (forward, reverse and symmetric) and the registration direction.

All the experiments were based on a multi-modality point-similarity measure with the similarity function:

$$f(\mathbf{i}) = \log \frac{p(\mathbf{i})^2}{p(i_A) \cdot p(i_B)}, \quad (17)$$

where the joint distribution $p(\mathbf{i})$ and the marginal distributions $p(i_A)$ and $p(i_B)$ are estimated from the images that are being registered. The registration was regularized using a Gaussian spatial deformation model (Rogelj et al., 2003) that follows the implementation of linear elasticity proposed by Bro-Nielsen (Bro-Nielsen, 1996).

Three different methods were used to assess the quality of the registration. First, when the correct transformation T_0 was known, the registration quality was measured directly by computing the RMS displacement error E_{RMS} ,

$$E_{RMS}(\mathbf{T}) = \sqrt{\frac{1}{N} \sum_{\mathbf{x}} (\mathbf{T}(\mathbf{x}) - \mathbf{T}_0(\mathbf{x}))^2} \quad (18)$$

where N is the number of image voxels. The second method measures the registration consistency by computing the RMS deviation of point correspondences defined by the transformations \mathbf{T} and \mathbf{T}' , which are obtained by registering the same images using the same method but in different registration directions.

$$C_{RMS}(\mathbf{T}, \mathbf{T}') = \sqrt{\frac{1}{N} \sum_{\mathbf{x}} (\mathbf{T}(\mathbf{x}) - \mathbf{T}'^{-1}(\mathbf{x}))^2} \quad (19)$$

\mathbf{T}'^{-1} denotes the inverse of transformation \mathbf{T}' , such that it forms the same image correspondence in the other registration direction. Please note that our symmetric registration approach does not enforce the inverse consistency, so it does make sense to verify by C_{RMS} measure whether the consistency in fact improves. The last method used for assessing the registration quality was the measurement of image similarity. This method is less appropriate (Woods, 1999) as it can only judge transformation components that change the image's appearance. For our experiments the correlation coefficient $CC(A, \mathbf{T}B)$, see (Hill and Hawkes, 1999), was used.

3.1 Registration of simple objects

Two images of simple objects were generated, a rectangular prism for image A and a sphere for image B . The central image slices are shown in Figure 8.

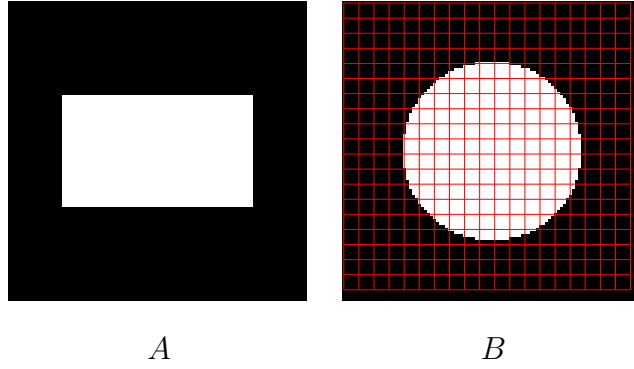


Fig. 8. The central slices of the simple 3D images, representing a rectangular prism (image A) and a sphere (image B). The lines in image B represent the image grid.

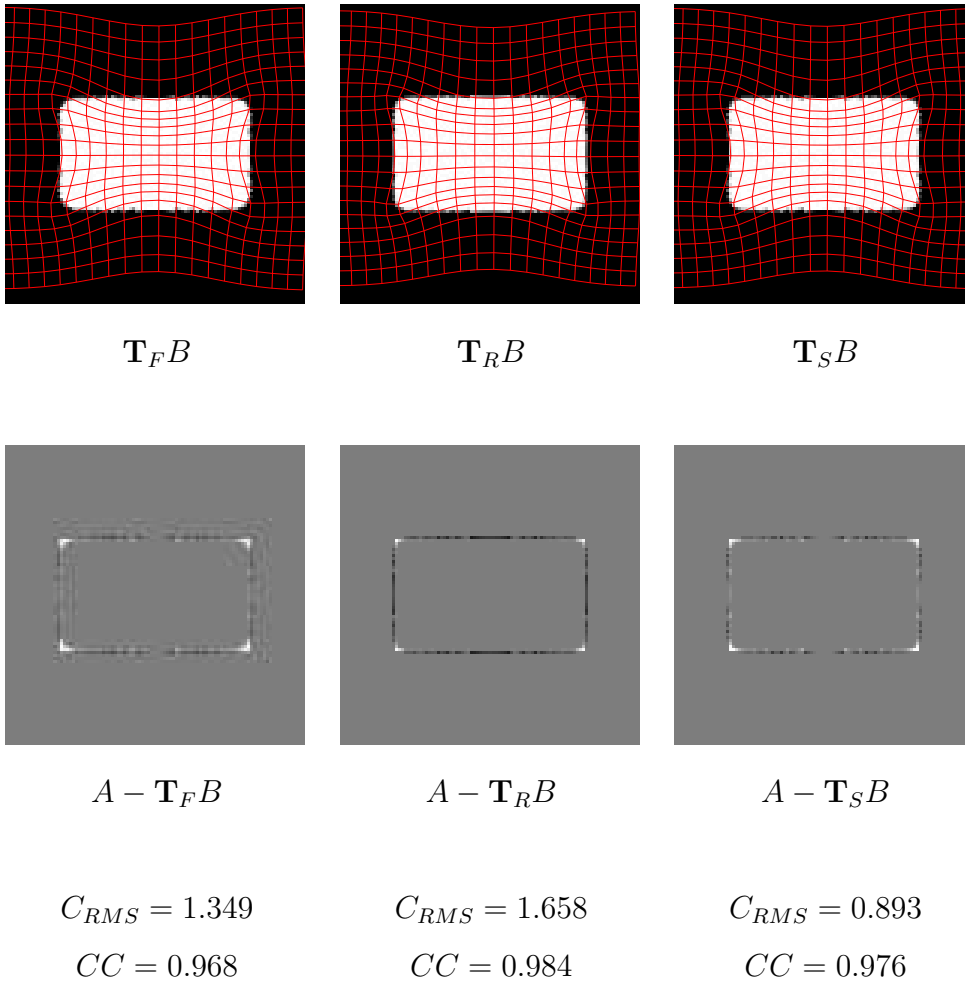


Fig. 9. Results of registering the simple image pair using different methods for estimating the external forces. The first row shows the resulting images $\mathbf{T}B$, and the second row shows the differences compared with the target image A . Below the images are the consistency results C_{RMS} and the final image similarities CC for each of the methods.

After registering the images with all three registration approaches in both directions, the results were compared by measuring the consistency C_{RMS} and the similarity of the registered images CC . As the ideal transformation \mathbf{T}_0 is not known in this case, the registration error E_{RMS} cannot be obtained.

The results are shown in Figure 9. Although all three resulting images look very similar, the consistency measure C_{RMS} indicates the advantage of the symmetric approach. The results of the other two methods are worse, especially when using only the reverse forces (transformation T_R). However, different conclusions could be drawn when observing the image similarity. Here, the method based on the reverse forces gives the best result, better than the symmetric approach. To find out which of the approaches is more correct we performed the second experiment, based on recovering synthetic deformations.

3.2 Recovering synthetic deformations

In this experiment we used Brainweb (Kwan et al., 1996) simulated images of a human head. First, the original MRI-T1 image was used for A , and its synthetically deformed version was used for B . Second, we performed a multi-modality registration by using the MRI-PD image as a target A , while B remained the same synthetically deformed MRI-T1 image, see Figure 10.

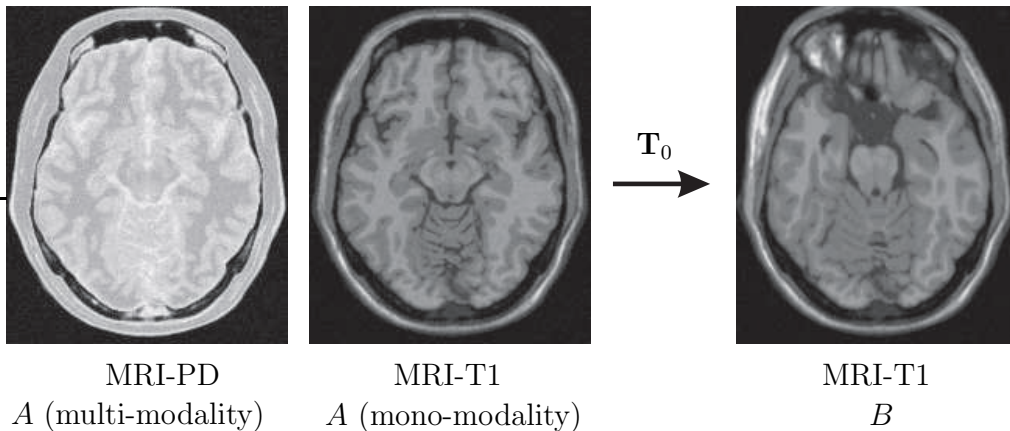


Fig. 10. Images used for the experiment based on recovering synthetic deformations. Image A was an original untransformed MRI-T1 image (mono-modality registration) or MRI-PD image (multi-modality registration). Image B was in all cases generated by deforming the original MRI-T1 image.

Five different synthetic deformations \mathbf{T}_0 were used, each of them generated as a sum of five three-dimensional Gaussian functions with randomly selected parameters, where the amplitude was in the range 0 to 26mm, and the standard deviation was in the range 5 to 50mm.

The synthetically generated transformation \mathbf{T}_0 made it possible to evaluate

Table 1
Results of recovering the synthetic deformations.

Experiment	Method	Mono-modality			Multi-modality		
		E_{RMS}	C_{RMS}	CC	E_{RMS}	C_{RMS}	CC
$\mathbf{T}_0^{(1)}$	\mathbf{T}_F	1.267	0.548	0.974	1.302	0.854	0.973
	\mathbf{T}_R	1.382	1.570	0.976	1.876	2.050	0.974
	\mathbf{T}_S	1.052	0.322	0.977	1.108	0.400	0.976
$\mathbf{T}_0^{(2)}$	\mathbf{T}_F	1.520	0.908	0.911	1.241	1.020	0.993
	\mathbf{T}_R	1.358	1.885	0.995	1.791	2.086	0.995
	\mathbf{T}_S	1.242	0.356	0.994	1.093	0.326	0.995
$\mathbf{T}_0^{(3)}$	\mathbf{T}_F	1.413	0.785	0.988	1.716	0.819	0.986
	\mathbf{T}_R	1.225	2.066	0.994	1.760	2.200	0.992
	\mathbf{T}_S	0.981	0.768	0.991	1.040	0.672	0.992
$\mathbf{T}_0^{(4)}$	\mathbf{T}_F	1.043	0.305	0.995	1.166	0.565	0.994
	\mathbf{T}_R	1.233	1.509	0.995	1.801	2.001	0.994
	\mathbf{T}_S	0.919	0.192	0.995	1.037	0.255	0.994
$\mathbf{T}_0^{(5)}$	\mathbf{T}_F	1.580	1.005	0.990	1.661	1.103	0.989
	\mathbf{T}_R	1.501	1.663	0.993	1.970	2.203	0.992
	\mathbf{T}_S	1.425	0.491	0.992	1.521	0.509	0.992
average	\mathbf{T}_F	1.578	0.916	0.987	1.417	0.872	0.987
	\mathbf{T}_R	1.489	1.731	0.991	1.840	2.108	0.989
	\mathbf{T}_S	1.330	0.510	0.990	1.160	0.433	0.990

the registration correctness E_{RMS} , the consistency C_{RMS} and the image similarity CC . Because the original MRI-T1 and MRI-PD images were registered, the measured CC and the original MRI-T1 image were also used to evaluate the multi-modality registration results ($\mathbf{T}B$). The results are tabulated in Table 1. In all cases the symmetric approach performed the best in terms of the registration correctness and the registration consistency, while the measurement of final image similarity gave similar results for all three registration approaches (considering the average initial image similarity $S_0 = 0.841$). It is also evident that the mono-modality and multi-modality registrations produce practically identical registration results.

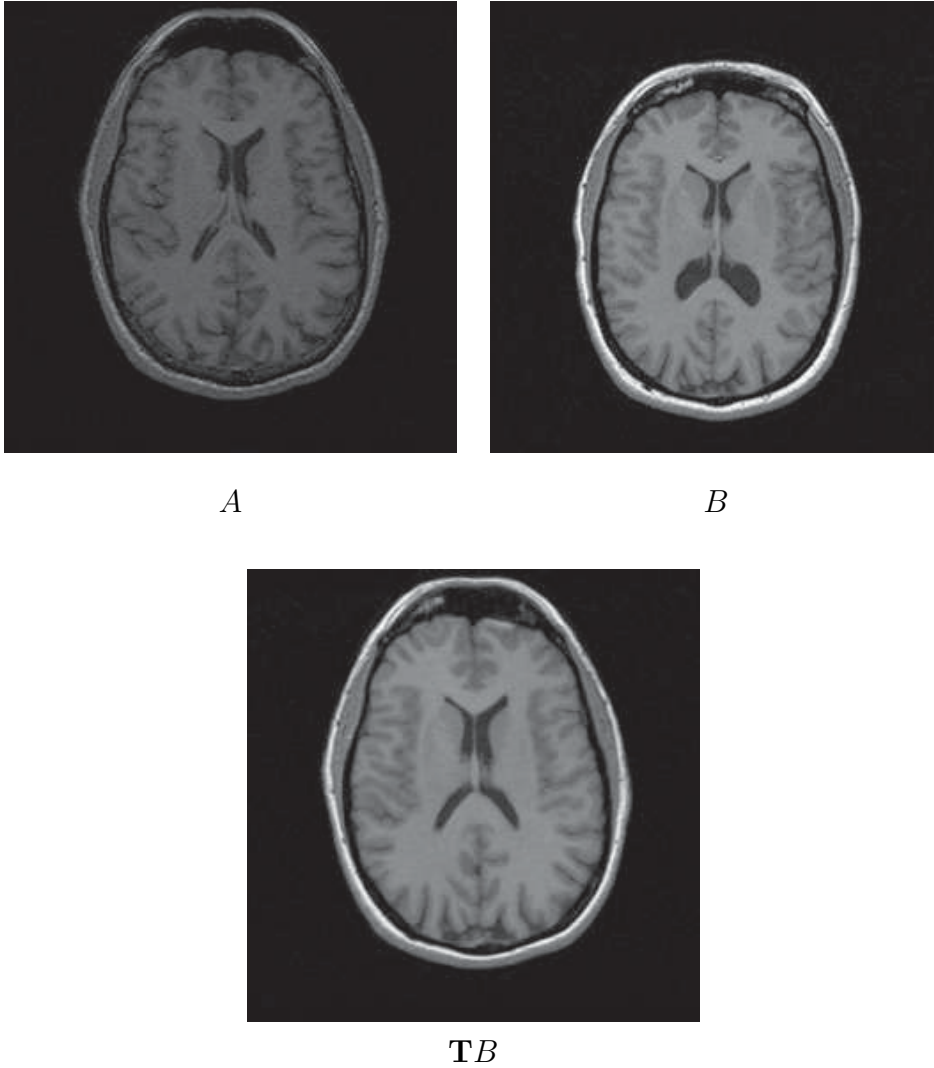


Fig. 11. An example of the inter-patient registration of real MRI-T1 images of a human head. Image A is a target used for registering image B , and TB is the registered image.

3.3 Registration of real inter-patient data

In the last experiment we tested how the symmetric registration approach performs in the case of real medical images and complex inter-patient transformations. We used six real MRI-T1 images of a human head. One image always served as image A and the other five images were used as image B . Thus, altogether there were five image pairs and each one of them was registered six times, by using all three different methods and registering in both directions. Example images are shown in Figure 11.

The registration results were evaluated by measuring the consistency C_{RMS} and the image similarity CC ; the registration error E_{RMS} cannot be measured

Table 2
Results of interpatient registration of real images of head.

Experiment	Method	C_{RMS}	CC
MRI01	\mathbf{T}_F	3.090	0.788
	\mathbf{T}_R	4.859	0.839
	\mathbf{T}_S	1.384	0.818
MRI02	\mathbf{T}_F	3.145	0.851
	\mathbf{T}_R	5.136	0.878
	\mathbf{T}_S	0.963	0.875
MRI03	\mathbf{T}_F	3.155	0.859
	\mathbf{T}_R	4.142	0.864
	\mathbf{T}_S	1.062	0.870
MRI04	\mathbf{T}_F	3.410	0.874
	\mathbf{T}_R	5.323	0.880
	\mathbf{T}_S	1.023	0.883
MRI05	\mathbf{T}_F	2.951	0.863
	\mathbf{T}_R	4.747	0.881
	\mathbf{T}_S	0.911	0.880
average	\mathbf{T}_F	3.150	0.847
	\mathbf{T}_R	4.841	0.868
	\mathbf{T}_S	1.068	0.865

due to the unknown ideal transformation \mathbf{T}_0 . The results are tabulated in Table 2.

It is clear that the consistency of the symmetric registration is, in all cases, much better than the consistency of the other two methods. As a result, we would expect that the results of the symmetric registration would also be more correct. However, it is also evident that the symmetric approach does not yield better results in terms of the final image similarity, which is similar for all three methods. This indicates that similarity measures are not capable of detecting the differences between the transformations obtained using different methods.

3.4 Discussion

All the results show that the symmetric registration approach performs better in terms of consistency than the standard registration approaches, thereby indicating a more correct registration. Furthermore, the results of recovering synthetic deformations prove that symmetric registration also improves the registration correctness. However, the improvement in the registration error is smaller than the improvement in the consistency, which indicates that some transformation components cannot be detected by measuring image similarity in any of the registration directions. Note that the gradients of similarity and the external forces still appear only at image points with a non-zero intensity gradient (although according to both images), which renders the exact registration of homogeneous image regions impossible. To improve the registration correctness of these regions an appropriate spatial deformation model must be used.

The results also show that in general the final image appearance becomes most similar to the target image when only the reverse forces are used. One possible explanation for this is that the reverse forces actually optimize the image similarity in the same registration direction as is observed after the images are registered.

In our implementation the reverse forces appear at the intensity gradients of the source image, while the forward forces appear at non-zero gradients of the target image. During the registration the image match changes from iteration to iteration and thus, forward forces appear at different coordinates with respect to the image that is being registered ($\mathbf{T}B$). This contributes to the registration consistency of the forward-force estimation method in comparison with the results for the reverse forces, see Table 2.

The consistency of the symmetric registration approach is considerably better than the consistency of the other two methods, although not as good as one would expect. We should emphasize that the differences between the results obtained in different registration directions are not caused only by the asymmetry of the similarity measurement, but also by the asymmetry of the spatial deformation model (Cachier and Rey, 2000). Two transformations of the same tissue, that are inverses of each other, generally require different deformation energies. This phenomenon arises because an additional deformation of already deformed tissue requires different energy than deformation of undeformed tissue. Registration tasks commonly assume that one of the images represents the undeformed state of the anatomy, while the other image represents the deformed anatomy. In this case it is important to know which image is playing which role, in order to correctly set the registration. Note that swapping of images, in order to perform registration in the opposite registra-

tion direction, also exchanges the assumptions of initial image deformations. Thus, if assumptions were correct for the original registration direction, they would be incorrect for the opposite direction, giving a raise to the registration error. This discrepancy of registration results obtained in both registration directions is also present in our experiments. As a consequence, the measure of consistency C_{RMS} loses its absolute meaning, because it does not measure only the disturbing asymmetry of similarity measurement, but also an eventually desirable asymmetry of the deformation model.

In contrast to *consistent image registration* (Christensen and Johnson, 2001) symmetric registration does not force the consistency. Instead, it improves the registration in one direction, without performing it in the opposite direction. As such it allows realistic asymmetric assumptions about the undeformed configuration of the anatomy and/or about the spatial deformation models. Furthermore, in comparison to the approach based on *inversion invariant energies* (Cachier and Rey, 2000) it only symmetrizes the *similarity energy* while not constraining the *regularization energies*. When the symmetrization of the *regularization energies* is also desired, this can be obtained by using the same spatial deformation model for both images. Finally, the implementation of symmetric registration is computationally efficient and does not require the computation of inverse transformations.

4 Conclusion

Symmetric image registration is a new aspect of the registration process. It is physically motivated and uses general physical laws. This solves the problem of the asymmetry of the similarity measurement, which is the main source of inconsistency and one of the sources of registration errors.

Three different experiments were performed to demonstrate the symmetric registration approach and to compare it with two standard unidirectional approaches. The results prove that the symmetric registration approach does improve the registration consistency as well as the registration correctness. In addition, the computational cost of the symmetric approach is still relatively low, as it does not require the computation of inverse transformations.

In general, the symmetric approach allows both images to be modeled by suitable deformable models and thus both of them could actually deform. Such an approach could better suit certain registration tasks when both of the images actually represent the deformed anatomy. In addition to this generalization, it would also be possible to use more than two images, which would interact with forces at the same time.

Finally, note that the registration process is completely symmetric only if both of the images are modeled using the same spatial deformation model. When this is not the case, the registration error depends on the selection of the registration direction and some inconsistency appears due to the different assumptions in the different registration directions.

References

- Ashburner, J., Andersson, J., Friston, K., 1999. High-dimensional nonlinear image registration using symmetric priors. *NeuroImage* 9, 619–628.
- Bajcsy, R., Kovačič, S., April 1989. Multiresolution elastic matching. *Computer Vision, Graphics and Image Processing* 46, 1–21.
- Bro-Nielsen, M., 1996. Medical image registration and surgery simulation. Ph.D. thesis, Department of Mathematical Modelling, Technical University of Denmark.
- Cachier, P., Rey, D., 2000. Symmetrization of the non-rigid registration problem using inversion-invariant energies : Application to multiple sclerosis. In: Delp, S. L., DiGioia, A. M., Jaramaz, B. (Eds.), *Proceedings of the 3rd International Conference on Medical Image Computing and Computer-Assisted Intervention – MICCAI 2000*. Vol. 1935 of *Lecture Notes in Computer Science*. Springer, pp. 472–481.
- Christensen, G., Johnson, H., July 2001. Consistent image registration. *IEEE Transactions on Medical Imaging* 20 (7), 568–582.
- Dengler, J., 1986. Local motion estimation with the dynamic pyramid. In: *The 8th International Conference on Pattern Recognition, ICPR86 (Paris)*. pp. 1289–1292.
- Fitzpatrick, J. M., 2001. Detecting failure, assessing success. In: Hajnal, J. V., Hill, D. L. G., Hawkes, D. J. (Eds.), *Medical Image Registration*. CRC Press, pp. 117–142.
- Gee, J. C., 2000. Performance evaluation of medical image processing algorithms. In: Hanson, K. (Ed.), *Medical Imaging 2000: Image Processing*. Vol. 3979 of *Proc. SPIE*. SPIE Press, Bellingham, WA, pp. 19–27.
- Hill, D. L. G., Hawkes, D. J., 1999. Across-modality registration using intensity-based cost functions. In: Bankman, I. (Ed.), *Handbook of Medical Image Processing*. Academic Press, pp. 537–553.
- Kwan, R.-S., Evans, A., Pike, G. B., May 1996. An extensible MRI simulator for post-processing evaluation. In: *Visualization in Biomedical Computing (VBC'96)*. Vol. 1131 of *Lecture Notes in Computer Science*. Springer-Verlag, pp. 135–140.
- Rogelj, P., Kovačič, S., 2003. Point similarity measure based on mutual information. In: Gee, J., Maintz, J., Vannier, M. (Eds.), *Biomedical Image Registration*. Vol. 2717 of *Lecture Notes In Computer Science (LNCS)*. Springer, pp. 112–121.

- Rogelj, P., Kovačič, S., Gee, J., October 2003. Point similarity measures for non-rigid registration of multi-modal data. *Computer vision and image understanding* 92 (1), 112–140.
- Schnabel, J. A., Tanner, C., Castellano-Smith, A. D., Degenhard, A., Leach, M. O., Hose, D. R., Hill, D. L. G., Hawkes, D. J., February 2003. Validation of nonrigid image registration using finite-element methods: application to breast MR images. *IEEE Transactions on Medical Imaging* 22 (3), 238–247.
- Woods, R., 1999. Validation of registration accuracy. In: Bankman, I. (Ed.), *Handbook of Medical Imaging Processing and Analysis*. Academic Press, pp. 491–497.